Assembly of thermally reduced graphene oxide nanostructures by alternating current dielectrophoresis as hydrogen-gas sensors

Jianwei Wang,[1] Budhi Singh,[1] Sunglyul Maeng,[2] Han-Ik Joh,[3] and Gil-Ho Kim[1,a)]
[1]*School of Electronic and Electrical Engineering and Sungkyunkwan Advanced Institute of Nanotechnology (SAINT), Sungkyunkwan University, Suwon 440-746, South Korea*
[2]*Department of Electronic and Electrical Engineering, Woosuk University, Wanju, Jeollabuk-do 565-701, South Korea*
[3]*Carbon Convergence Materials Research Center, Institute of Advanced Composite Materials, Korea Institute of Science and Technology, San 101, Eunha-ri, Bongdong-eup, Wanju-gun, Jeollabuk-do 565-905, South Korea*

(Received 1 July 2013; accepted 29 July 2013; published online 22 August 2013)

Chemo-resistive hydrogen-gas sensors based on thermally reduced graphene oxide (rGO) have been fabricated on a micro-hotplate by positive ac dielectrophoresis (DEP). The optimized DEP parameters for manipulating rGO nanostructures into Au electrodes for hydrogen sensing are: applied frequency = 1 MHz, peak-to-peak voltage = 5 V, and DEP time = 30 s. The device exhibits good sensitivity (~6%) with fast response time (~11 s) and recovery time (~36 s) for 200 ppm hydrogen gas at room temperature. This result indicates that the DEP process has great potential for assembling rGO for hydrogen-gas sensor in many industrial and scientific applications.
 [http://dx.doi.org/10.1063/1.4819378]

Hydrogen as an energy carrier exhibits excellent properties and is recognized as a clean and renewable alternative to carbon-based fuels.[1] Hydrogen is environmentally friendly, its only by-product being water. However, hydrogen gas is inflammable and easily combusts in air at a concentration of approximately 4%. Therefore, the demand for a highly sensitive, selective, and stable hydrogen-gas sensor has increased because of its application in (i) petroleum transformation, (ii) cryogenic cooling, (iii) chemical processing, (iv) rocket engines, and (v) fuel cell technology. One-dimensional nanostructures such as carbon nanotubes and metal oxide nanowires have been extensively used for gas sensing because of their excellent sensitivity, selectivity, and stability.[2–4] At present, a great deal of research is being conducted on graphene-based sensors.[5–7] Its two-dimensional honeycomb structure, excellent conductivity, and high surface-to-volume ratio make graphene a suitable candidate for future gas-sensing applications. Gaseous molecules that adsorb/desorbs on the graphene surface act as donors or acceptors, changing the conductance of graphene. However, graphene does not have very good gas sensitivity because of the absence of dangling bonds from its surface, which are required for the adsorption of gas molecules. The response of a graphene gas sensor can be improved by functionalizing it with carboxyl, epoxy, hydroxyl, and carbonyl groups.

The functionalized graphene oxide (GO) nanostructures were synthesized by a modified Hummers method in which 4 g of graphite flakes were added to a 250-ml round-bottom flask containing 120 ml of H_2SO_4 and then stirred for 1 h. $KMnO_4$ aqueous solution was added to the mixture at 20 min intervals with stirring. The mixture was slowly heated to 40 °C and maintained this temperature for 5 h to oxidize the graphite. Subsequently, 150 ml of deionized (DI) water was added to the mixture. Next, 17 ml of H_2O_2 solution was added to the mixture under stirring for 30 min and then held at this condition for 24 h after which the mixture was centrifuged. The mixture was enclosed in a dialysis tube washed several times with ultrapure DI water to obtain a pH level of 5. Finally, the graphene oxide was dried in a freeze dryer at −60 °C for 48 h.[6,8]

The GO is electrically insulating, but its conductivity can be increased to up to 10^4 times by exposing it to reducing agents such as hydrazine, $NaBH_4$, or via the temperature treatment.[9,10] However, chemical reducing agents such as hydrazine are toxic, environmentally hazardous, and contaminate the resulting material. In addition, they introduce extra nitrogen functional groups on the graphene sheets, which may slow down the sensing response. In this letter, we report the fabrication of high-performance hydrogen-gas sensors using GO, which is partially reduced by low-temperature annealing in vacuum.

An X-ray Diffraction (XRD) study was carried using a PANalytical XPert Pro X-ray diffractometer with nickel-filtered Cu K_α radiation as the X-ray source. The samples were scanned in steps of 0.02° in the 2θ range of 5°–20°. The chemical bonding characteristics of the GO nanostructures were examined by XPS (ESCA 2000, VG Microtech, UK) using twin anode X-ray source Al K_α (1486.6 eV)/Mg K_α (1253.6 eV) under a vacuum of 10^{-9} Torr. The Raman spectra were acquired with a WITec Raman microscope with a 532 nm laser. The sensing properties of the GO nanostructure device were analyzed in a vacuum chamber by observing the change in the conductance with and without hydrogen gas flow. Current-voltage (I-V) characteristics of the GO nanostructures between Au electrodes were investigated using an I-V measurement system (Keithley, Model 4200-FCS).

The sensing device was fabricated by assembling the reduced GO (rGO) nanostructures onto a micro-hotplate by ac dielectrophoresis (DEP). Figure 1(a) shows the schematic

a)Email: ghkim@skku.edu

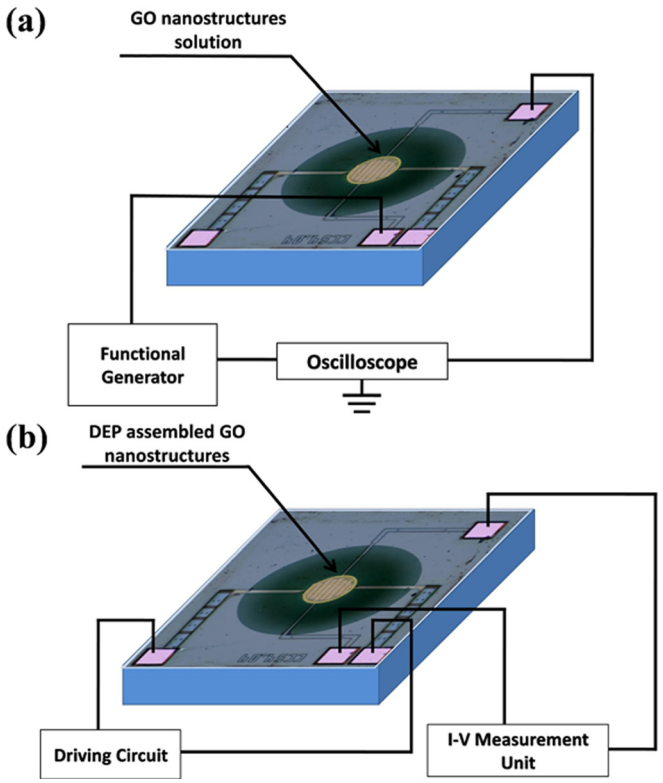

FIG. 1. Schematic representation of experimental setup used for (a) DEP of rGO nanostructures into Au electrodes, and (b) hydrogen-gas sensing at different operating temperatures. Driving circuit maintains the temperature of the micro-hotplate.

representation of the experimental setup used for an ac DEP assembly, which consists of a function generator connected directly and through a chip to the oscilloscope. The micro hotplate were composed of 150 μm diameter integrated electronic devices (IEDs) and heaters, which can attain a maximum temperature of 600 °C. The operating temperature of the rGO sensor is varied using the heater and recorded by a thermocouple connected to a digital display multimeter. Figure 1(b) shows the schematic representation of the experimental setup for the sensing measurement. A driving circuit is used to maintain the temperature of the micro-hotplate.

Figure 2(a) shows the typical XRD pattern of the GO and rGO nanostructures. The (002) peak, which is characteristic of the GO nanostructure, is located at approximately 11.8° corresponding to an interlayer distance at ~0.7 nm. The XRD pattern of the rGO shows a diffraction peak at approximately 23.4° that corresponds to an interlayer spacing distance of 0.4 nm. The shifting of the peak toward a higher angle after reduction is because of the removal of the oxygen atoms from the GO nanostructures.[6,9] The XPS analysis was performed to elucidate the surface features and chemical states of GO and rGO nanostructures. Figure 2(b) shows the characteristic peaks of C = C/C-C (284.6 eV), C-N (286.7 eV), C-O/C-O-C or hydroxyl and epoxy (288.4 eV), and the carboxyl group (290.6 eV). It was observed that all the oxygen-containing functional groups had been removed in the case of rGO. This indicates loss of oxygen and formation of a sp^2 carbon domain after the reduction process. The XPS spectra of GO (inset of Figure 2(b)) indicate that GO contains a larger amount of hydroxyl groups than the sp^2-hybridized carbon.[6,11]

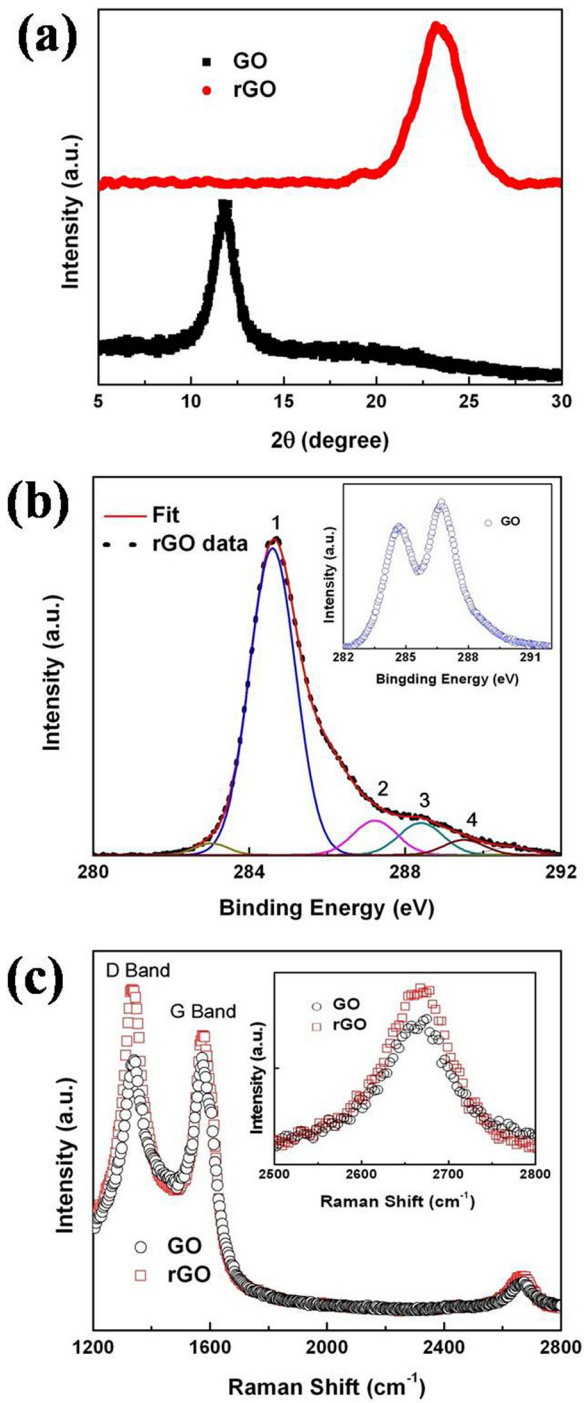

FIG. 2. (a) X-ray diffraction patterns of GO and rGO nanostructures indicating shifts in 2θ (002) peak toward higher diffraction angle because of thermal reduction in vacuum. (b) XPS data of C1s peak of rGO nanostructures with levels 1–4 denote peaks of sp^2-hybridized carbon, hydroxyl, epoxide, and carboxyl functional groups. Inset shows the XPS spectrum of GO nanostructures. (c) Raman spectra of GO and rGO nanostructures with D, G, and 2D bands. Inset shows enlarged version of 2D band of GO and rGO nanostructures.

Figure 2(c) shows the Raman spectra of the GO and rGO nanostructures. The most prominent peaks observed in rGO and GO are the D band at 1336 cm^{-1} and the G band at 1564 cm^{-1}. The G band occurs because of the optically allowed E_{2g} mode and represents the in-plane vibrations of the graphitic carbon. The small red shift of the G band in the rGO indicates that the electrons trapped by the various

functional groups in GO are freed in rGO, leading to an increase in free-electron density.[12] The presence of D band indicates the amount of imperfections present on the carbon basal plane due to the attachment of the hydroxyl and epoxide groups. The I_D/I_G ratio in rGO is larger than that in GO indicating that the reduction process altered the structure of GO giving rise to a great deal of defects. A similar behavior was observed by Moon *et al.* for rGO reduced by chemical graphitization.[13] The inset of Figure 2(c) shows the enlarged view of the 2D band of GO and rGO at 2700 cm^{-1}. This band is associated with two in-plane transverse optical phonons at the K and K′ points. Higher intensity of 2D band in rGO compared to that in GO also indicates that reduction alters the structure of GO.[12]

DEP allows the selective deposition or directed movement of spherical and one-dimensional micro- and nanoscale objects in nonuniform electric fields. This includes polymer particles, cells, DNA, nanowires, bundles, or individual carbon nanotubes for the characterization of physical properties.[14–21] The DEP force, $\vec{F}_{DEP} = (\vec{p}.\vec{\nabla})\vec{E}$, is exerted on an induced dipole moment $\vec{p}$ of polarizable particles in a nonuniform electric field. In general, the time-averaged DEP force experienced by a nanoparticle is expressed as $\vec{F}_{DEP} = 2\pi\varepsilon_m R^3 Re[K(\omega)]\nabla E^2_{rms}$, where ε_m is the permittivity of the medium, R is the radius of the nanoparticle, $K(\omega)$ is the Clausius-Mossotti factor, and E_{rms} is the rms value of the electric field.[22,23] The frequency-dependent behavior exists in the Clausius-Mossotti factor $K(\omega)$, which represents the complex polarizability of the nanostructures and is given by

$$K(\omega) = \frac{\varepsilon_p - \varepsilon_m - \left(\frac{j}{\omega}\right)(\sigma_p + \sigma_m)}{\varepsilon_p - 2\varepsilon_m - \left(\frac{j}{\omega}\right)(\sigma_p + 2\sigma_m)}, \quad (1)$$

where ε_p and ε_m are the permittivities of the particle and medium, ω is the angular frequency, σ_p and σ_m are the conductivities of the particles and medium. Solving Eq. (1) for the real part of $K(\omega)$, we have

$$Re[K(w)] = \frac{(\varepsilon_p - \varepsilon_m)(\varepsilon_p + 2\varepsilon_m) + \left(\frac{1}{\omega^2}\right)(\sigma_p - \sigma_m)(\sigma_p + 2\sigma_m)}{(\varepsilon_p + 2\varepsilon_m)^2 + \left(\frac{1}{\omega^2}\right)(\sigma_p + 2\sigma_m)^2}. \quad (2)$$

DEP can be either positive or negative. Positive DEP occurs when the $Re[K(w)]$ has a positive value where a time-averaged force pulls the nanoparticles toward the field of strong electric field. A negative value of $Re[K(w)]$ causes negative DEP and corresponds to a negative averaged force, directing the nanoparticles toward the field of weak electric field. Figure 3 shows the variation of $Re[K(w)]$ with frequency using the conductivities and permittivities of the rGO nanostructures ($\sigma_p = 300\,Scm^{-1}$, $\varepsilon_p = 3.5\varepsilon_0$) and the medium DI water ($\sigma_m = 1\,Scm^{-1}$, $\varepsilon_m = 80\varepsilon_0$).[24,25] In the next paragraph, we show that the optimized frequency used for the rGO DEP is toward positive DEP.

To achieve the successful assembly of the rGO nanostructures on the micro-hotplate, it is important to optimize

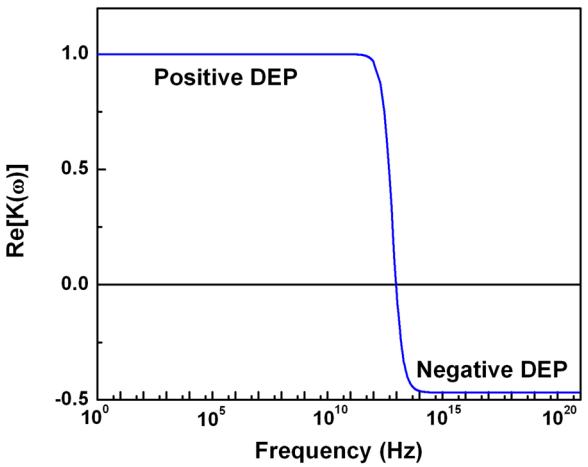

FIG. 3. Real part of Clausius-Mossotti factor $Re[K(\omega)]$ versus frequency for rGO nanostructures in water.

the DEP parameters, i.e., frequency of the applied signal, peak-to-peak voltage (V_{pp}), and duration of the DEP process. Figure 4 shows the current-voltage characteristics of the rGO sensor at various DEP parameters. It has been found that DEP of rGO at 1 MHz, 10 V, 30 s and 1 MHz, 5 V, 60 s does not show any measurable current for hydrogen-sensing applications. This is because the 2-μm-gap Au electrodes may get burnt at higher applied voltage (or for longer DEP duration), which reduces the ability to manipulate rGO between the electrodes. It is also observed that the conductance of the device increases when the applied frequency increases from 100 kHz to 1 MHz by maintaining V_{pp} at 5 V and DEP time at 30 s. This increase in conductance with frequency indicates that the assembly of the rGO nanostructures at 1 MHz frequency is more reliable and consistent. The device fabricated at low $V_{pp} = 2$ V (applied frequency = 1 MHz, DEP time = 30 s) and a smaller DEP duration of 10 s (applied frequency = 1 MHz, $V_{pp} = 5$ V) shows a current that is approximately less than an order of magnitude when compared to the device fabricated at 1 MHz, 5 V, and 30 s. This may be because of the fact that at lower V_{pp} (or for smaller

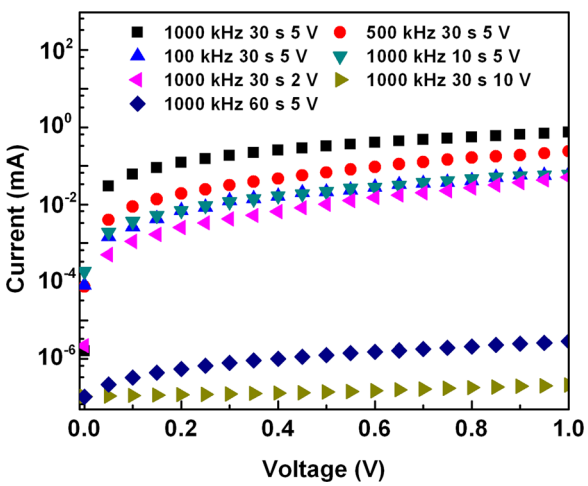

FIG. 4. Current-voltage characteristics of rGO hydrogen-gas sensors at different DEP parameters: (a) 1 MHz, 30 s, 5 V; (b) 500 kHz, 30 s, 5 V; (c) 100 kHz, 30 s, 5 V; (d)1 MHz, 10 s, 5 V; (e) 1 MHz, 30 s, 2 V; (f) 1 MHz, 30 s, 10 V; and (g) 1 MHz, 60 s, 5 V.

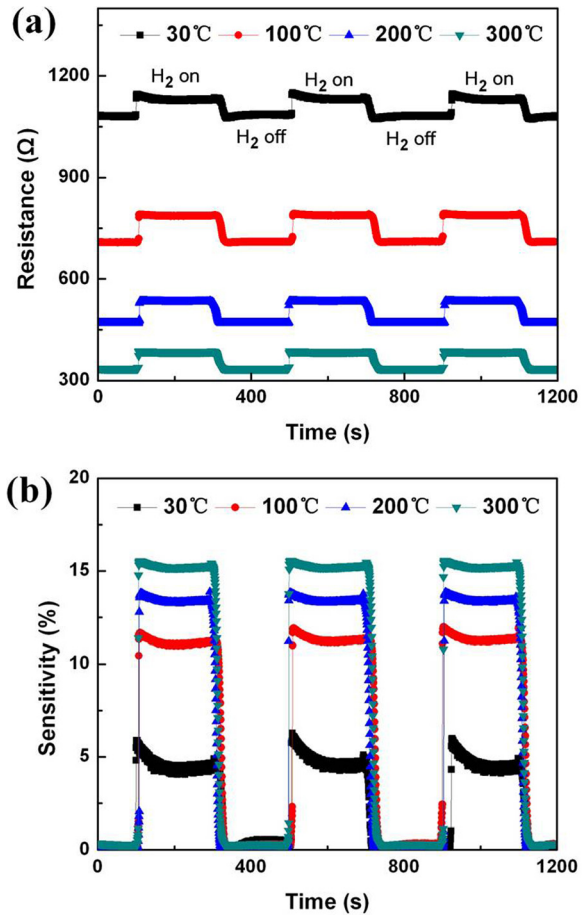

FIG. 5. (a) Change in resistance of rGO sensor for 200 ppm hydrogen gas at various operating temperatures. (b) Sensitivity of rGO sensors at different operating temperatures for 200 ppm hydrogen gas.

duration), a less significant rGO channel or current path is formed between the Au electrodes. Therefore, current-voltage measurements at different DEP parameters suggest that rGO DEP at 1 MHz, 5 V, and 30 s is most suitable for fabricating hydrogen-gas sensor on a micro-hotplate.

Figure 5(a) shows the resistance behavior of the rGO gas sensor when intermittently exposed to 200 ppm hydrogen gas at various operating temperatures. The resistance of rGO increases when exposed to hydrogen gas; this indicates that rGO is a *p*-type semiconductor where shallow donor levels do not exist.[6] The resistance of the rGO decreases when the operating temperature increases from 30 to 300 °C. A low resistance of approximately 1 kΩ at room temperature indicates the presence of a significant amount of rGO, which agrees well with the XPS data. Figure 5(b) shows the sensitivity of rGO to 200 ppm hydrogen gas under various temperature conditions. The sensitivity of a gas sensor is defined as $\Delta R/R(\%) = (R - R_0)/R_0 \times 100$, where R_0 represents the baseline resistance and R represents the resistance of the device when exposed to hydrogen gas. The sensitivity of the rGO sensor tends to increase from 6% to 17% as the operating temperature increase from 30 to 300 °C. This result demonstrates that the DEP-fabricated rGO-based hydrogen-gas sensor exhibits fairly good sensitivity at room temperature compared to a device fabricated by the drop-coating method.[6]

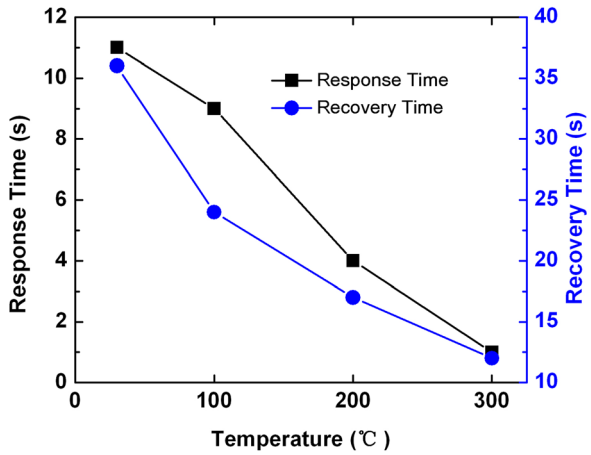

FIG. 6. Response and recovery time of rGO sensor for 200 ppm hydrogen gas at different operating temperatures.

Figure 6 shows the dependence of the response and recovery time of the sensing device for 200 ppm hydrogen gas at different operating temperatures. The response time decreases and the recovery times increase with operating temperature. At room temperature, the response and recovery times are ∼11 s and ∼36 s, respectively. The sensor operation at 300 °C is ideal as both the sensitivity (∼17%) and response time (∼1 s) are very good. However, operation of the hydrogen sensor at high temperatures is a problem with regard to both economy and safety; hence, room-temperature operation is highly desirable. The fairly good sensitivity (∼6%)with fast response time (∼11 s) and recovery time (∼36 s) at room temperature are adequate for hydrogen-gas monitoring in various industrial and scientific applications.

In conclusion, we fabricated a practical *p*-type hydrogen-gas sensor using thermally reduced GO by the DEP process on a micro-hotplate with 2-*μ*m-gap Au electrodes. The DEP parameters are optimized in order to assemble the rGO between the Au electrodes in a precise manner. The sensitivity of the sensor is 6% at room temperature with a fast response (∼11 s) and recovery time (∼36 s) that is adequate for the detection of hydrogen gas in scientific research and industrial applications. The real part of Clausius-Mossotti factor *Re* [*K* (*ω*)] versus frequency indicates a reliable and consistent assembly of rGO nanostructures between the conducting electrodes by positive DEP. The XRD, XPS, and Raman spectroscopy analyses were conducted to investigate the structural and functional properties of the rGO nanostructures used. This work indicates that DEP is an effective approach to assemble the rGO nanostructures in a precise manner compared to the drop-dried process.

This research was supported by the Basic Science Research Program through the National Research Foundation of Korea (NRF), funded by the Ministry of Education, Science and Technology (2012R1A1A2042230 and R32-10204).

[1]G. W. Crabtree, M. S. Dresselhaus, and M. V. Buchanan, Phys. Today **57**(12), 39 (2004).
[2]J.-W. Han, B. Kim, J. Li, and M. Meyyappan, Appl. Phys. Lett. **102**, 193104 (2013).

[3]J. Y. Luo, X. X. Chen, W. D. Li, W. Y. Deng, W. Li, H. Y. Wu, L. F. Zhu, and Q. G. Zeng, Appl. Phys. Lett. **102**, 113104 (2013).
[4]J. M. Baik, M. H. Kim, C. Larson, C. T. Yavuz, G. D. Stucky, A. M. Wodtke, and M. Moskovits, Nano Lett. **9**, 3980 (2009).
[5]F. Yavari, E. Castilo, H. Gullapalli, P. M. Ajayan, and N. Koratkar, Appl. Phys. Lett. **100**, 203120 (2012).
[6]J. Wang, Y. Kwak, I.-Y. Lee, S. Maeng, and G.-H. Kim, Carbon **50**, 4061 (2012).
[7]W. Yuan, A. Liu, L. Huang, C. Li, and G. Shi, Adv. Mater. **25**, 766 (2013).
[8]M. Hirata, T. Gotou, S. Horiuchi, M. Fujiwara, and M. Ohba, Carbon **42**, 2929 (2004).
[9]C. Gomez-Navarro, R. T. Weitz, A. M. Bittner, M. Scolari, A. Mews, M. Burghard, and K. Kern, Nano Lett. **7**, 3499 (2007).
[10]T. V. Cuong, V. H. Pham, E. W. Shin, J. S. Chung, S. H. Hur, E. J. Kim, Q. T. Tran, H. H. Nguyen, and P. A. Kohl, Appl. Phys. Lett. **99**, 041905 (2011).
[11]S. Yumitori, J. Mater. Sci. **35**, 139 (2000).
[12]J. Lim, K. Choi, J. R. Rani, J.-S. Kim, C. Lee, J. H. Kim, and S. C. Jun, J. Appl. Phys. **113**, 183502 (2013).
[13]I. K. Moon, J. Lee, R. S. Ruoff, and H. Lee, Nat. Commun. **1**, 73 (2010).
[14]H. A. Pohl, J. Appl. Phys. **22**, 869 (1951).
[15]H. A. Pohl and I. Hawk, Science **152**, 647 (1966).
[16]J. F. Conley, L. Stecker, and Y. Ono, Appl. Phys. Lett. **87**, 223114 (2005).
[17]M. Washizu and O. Kurosawa, IEEE Trans. Ind. Appl. **26**, 1165 (1990).
[18]L. Zheng, S. Li, J. P. Brody, and P. J. Burke, Langmuir **20**, 8612 (2004).
[19]P. A. Smith, C. D. Nordquist, T. N. Jackson, T. S. Mayer, B. R. Martin, J. Mbindyo, and T. E. Mallouk, Appl. Phys. Lett. **77**, 1399 (2000).
[20]K. Yamamoto, S. Akita, and Y. Nakayama, Jpn. J. Appl. Phys., Part 1 **35**, 917 (1996).
[21]X. Q. Chen, T. Saito, H. Yamada, and K. Matsushige, Appl. Phys. Lett.**78**, 3714 (2001).
[22]B. C. Gierhart, D. G. Howitt, S. J. Chen, R. L. Smith, and S. D. Collins, Langmuir **23**, 12450 (2007).
[23]P. R. C. Gascoyne and J. Vykoukal, Electrophoresis **23**, 1973 (2002).
[24]S. Pei, J. Zhao, J. Du, W. Ren, and H.-M. Cheng, Carbon **48**, 4466 (2010).
[25]T. S. Bui, J. Kim, E. Jung, H. S. Le, N. T. Nguyen, and J.-Y. Bae, Displays **34**, 192 (2013).